Available online at www.sciencedirect.com
ScienceDirect
Trans. Nonferrous Met. Soc. China 30(2020) 3031−3042
Transactions of Nonferrous Metals Society of China
www.tnmsc.cn

Flow stress prediction of Hastelloy C-276 alloy using modified Zerilli−Armstrong, Johnson−Cook and Arrhenius-type constitutive models

Yu LIU[1,2], Ming LI[1], Xian-wei REN[1], Zheng-bing XIAO[1,3], Xie-yi ZHANG[1], Yuan-chun HUANG[1,2,3,4]

1. Research Institute of Light Alloy, Central South University, Changsha 410083, China;
2. Nonferrous Metal Oriented Advanced Structural Materials and Manufacturing Cooperative Innovation Center, Central South University, Changsha 410083, China;
3. State Key Laboratory of High performance Complex Manufacturing, Central South University, Changsha 410083, China;
4. School of Mechanical and Electrical Engineering, Central South University, Changsha 410083, China

Received 30 January 2020; accepted 17 September 2020

Abstract: To better understand the hot deformation behaviors of Hastelloy C-276 alloy under elevated temperatures, hot tensile tests were carried out in the temperature range of 1223−1423 K and the strain rate range of 0.01−10 s^{-1}, respectively. Based on the modified Zerilli−Armstrong, modified Johnson-Cook, and strain-compensated Arrhenius-type models, three constitutive equations were established to describe the high-temperature flow stress of this alloy. Meanwhile, the predictability of the obtained models was evaluated by the calculation of correlation coefficients (r) and absolute errors (Δ), where the values of r for the modified Zerilli−Armstrong, Johnson−Cook, and Arrhenius-type constitutive models were computed to be 0.935, 0.968 and 0.984, and the values of Δ were calculated to be 13.4%, 10.5% and 6.7%, respectively. Moreover, the experimental and predicted flow stresses were compared in the strain range of 0.1−0.5, the results further indicated that the obtained modified Arrhenius-type model possessed better predictability on hot flow behavior of Hastelloy C-276.

Key words: Hastelloy C-276 alloy; hot tensile behaviors; constitutive models; flow stress

1 Introduction

Hastelloy C-276 alloy, a Ni−Cr−Mo superalloy, has been widely used in oil, chemical and nuclear industries for its high elevated temperature strength, good resistance to neutron radiation and excellent anti-oxidation ability [1,2]. As well recognized, the mechanical behaviors of metals and alloys are closely related to their hot forming process [3], during which the materials are subjected to complex strains, strain rates and temperatures. Thus, to better design and optimize the processing technology of a specific member, it is of great importance to understand the underlying deformation behaviors of metals and alloys [4]. In this regard, numerical simulation offers an effective approach to predict deformation behaviors and has been successfully applied to instructing extrusion, rolling and forging technologies of metallic materials [5,6].

For the numerical simulation model, the constitutive equation that describes the flow behaviors of materials is a critical input to simulate the deformation behaviors of materials under specified loading conditions [7,8]. It is well accepted that the reliability of the numerical simulation results is largely dependent on the accuracy of the constitutive equation which describes the flow

Foundation item: Project (ZZYJKT2018-06) supported by the State Key Laboratory of High Performance Complex Manufacturing of Central South University, China; Project (2019zzts525) supported by the Fundamental Research Funds for the Central Universities of Central South University of China

Corresponding author: Yuan-chun HUANG; Tel: +86-731-88877315; E-mail: science@csu.edu.cn

DOI: 10.1016/S1003-6326(20)65440-1

stresses. In the past years, several constitutive models were proposed to describe the deformation behaviors of metallic materials, which mainly include physically-based models, and empirical or semi-empirical models [9,10]. The physically-based models (such as MTS model and BCJ model [11]) can be built based on the experimental data, and the obtained models can predict the deformation behavior over a wide range of temperatures and strain rates accurately [12]. However, to establish such a physically-based constitutive equation is always time-consuming and expensive, as a large number of experimental data were needed. Accordingly, the empirical or semi-empirical models were highly developed for their simple manner, and the Johnson-Cook (JC) [13], Zerilli−Armstrong (ZA) [14] and Arrhenius type constitutive models [15] are three popular examples that have been widely used in numerical simulation softwares.

The JC model has been applied in many finite element analysis cases to predict the hot deformation behavior of alloys for its simple multiplication form [16,17]. However, the prediction accuracy of original JC model is limited by lacking of considering the comprehensive impact of temperatures, strains and strain rates on the flow behavior of materials [18]. Therefore, it has been revised several times by considering the effect of adiabatic temperature rise and strain rate sensitivity during material deformation [19−21]. The ZA model was also used to describe the deformation behaviors of materials under different strain rates and temperatures [22,23]. Based on the original ZA model, SAMANTARAY et al [24] developed a modified model by taking into account the influence of thermal softening, strain-state hardening and isotropic hardening, as well as the coupled impacts of temperature, strain and strain-rate on flow stresses, and the flow behaviors of modified 9Cr−1Mo steel under elevated temperatures were accurately predicted with this model. Moreover, the Arrhenius type constitutive model, proposed by SELLARS and MCTEGART [15], has been successfully applied to predicting the flow behavior of metals at elevated temperatures. In the original model, the flow stress is expressed by the sine-hyperbolic law in an Arrhenius type equation, and several modified models have been proposed to depict the flow behavior for different alloys at elevated temperatures. SLOOFF et al [25] revised the model by introducing a strain-dependent parameter into the hyperbolic sine constitutive equation, which turned out to well predict the flow behavior of a wrought magnesium alloy. Meanwhile, LIN et al [26] proposed a strain and strain-rate compensation method to this model, and the flow behaviors of 42CrMo steel were well described under different deformation temperatures and strain rates with the modified model. Furthermore, this modified model was also successfully employed to predict the flow behaviors of hot deformation in many other metals and alloys [27,28].

Meanwhile, KONG et al [29] reported the hot deformation characteristics and processing map of nickel-based C-276 superalloy using the hot compression test in the temperature range of 950−1250 °C with the strain rate range of 0.01−10.0 s^{-1}. In addition, based on the hot compression tests in the temperature range of 1000−1200 °C with the strain rate range of 0.01−10.0 s^{-1}, ZHANG et al [30−32] characterized the hot deformation behavior, dynamic recrystallization and microstructure evolution of Hastelloy C-276 using constitutive equation and processing map. LU et al [33] studied the hot tensile behavior of C-276 superalloy in the deformation temperature range of 650−750 °C with the strain rate range of 0.35−35 mm/s. As can be seen, many reported works on Hastelloy C-276 alloy were focused on the flow behaviors under hot compression, studies on the hot tensile behaviors of this alloy at elevated temperatures are still limited. Thus, to fully understand the hot deformation behavior of this alloy, the hot tensile deformation behaviors of Hastelloy C-276 alloy in the temperature range of 1223−1423 K and the strain rate range of 0.01−10 s^{-1} are studied in this work. The modified Johnson−Cook, Zerilli–Armstrong and Arrhenius-type constitutive models are established to predict the hot tensile behaviors of this alloy, also, a comparative study was performed to evaluate the prediction accuracy of the three established models by calculating the correlation coefficients and absolute errors.

2 Experimental

In the present study, Hastelloy C-276 alloy

with a chemical composition (wt.%) of 15.49Cr−15.45Mo−6.41Fe−3.57W−0.55Mn−0.236V−0.26Co−0.23Si−Ni(Bal.) was used for the experiments. According to ISO 783—1999, the tensile specimens, tested on a Gleeble−3500 thermo-simulation machine, were machined from a cold-rolled sheet with a thickness of 2 mm. Firstly, the specimens were solution treated at 1393 K for 30 min, and subsequently quenched by water to room temperature before testing. Secondly, the specimens were reheated to the testing temperature at a heating rate of 10 K/s, and held for 3 min to eliminate the thermal gradients on the whole specimen. The testing temperatures were in the range of 1223−1423 K at an interval of 100 K, and the strain rates were set to be 0.01, 0.1, 1, and 10 s^{-1}, respectively. After the specimens were completely cracked, samples were quickly cooled to room temperature with liquid nitrogen.

3 Results and discussion

3.1 Strain and stress curves of tensile testing

Figure 1 presented the strain−stress curves at 1423 K with different strain rates and at 0.01 s^{-1} with different deformation temperatures. As can be seen, the peak stress of Hastelloy C-276 alloy was significantly decreased with increasing deformation temperature or lowering strain rates, also the flow behaviors of this alloy were quite different under different deformation conditions. In this work, we mainly interested in the plastic deformation stage, as the relatively steady-state presented in the strain range of 0.1−0.5. In particular, it has been widely reported that this steady-state plays an important role in understanding the whole deformation process in metals and alloys [19,21]. Thus, in the following studies, the constitutive equations were built based on the true strain and stress in the deformation strain range of 0.1−0.5.

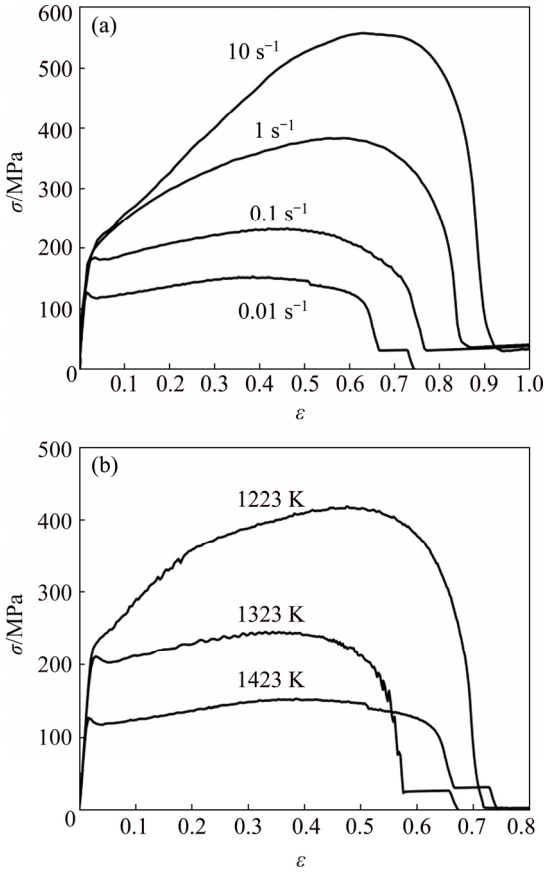

Fig. 1 Typical strain−stress curves of Hastelloy C-276 alloy at 1423 K (a) and at 0.01 s^{-1} (b)

3.2 Constitutive equations for predicting flow stress of Hastelloy C-276 alloy

3.2.1 Modified Zerilli−Armstrong model

The modified Zerilli−Armstrong model can be expressed as [14]

$$\sigma = (C_1 + C_2\varepsilon^n)\exp[-(C_3 + C_4\varepsilon)T^* + (C_5 + C_6T^*)\ln\dot{\varepsilon}^*] \quad (1)\#$$

where C_1, C_2, C_3, C_4, C_5, C_6 and n are material constants; σ and ε are flow stress and equivalent plastic strain, respectively; T and T_{ref} are deformation temperature and reference temperature, and $T^*=T-T_{ref}$, $\dot{\varepsilon}$ and $\dot{\varepsilon}_0$ are strain rate and reference strain rate, and $\dot{\varepsilon}^*=\dot{\varepsilon}/\dot{\varepsilon}_0$. In the present study, 1223 K and 0.01 s^{-1} were selected as reference temperature and reference strain rate, respectively, to determine the material constants.

When $\dot{\varepsilon}=\dot{\varepsilon}_0$=0.01 s^{-1}, Eq. (1) can be written as

$$\sigma = (C_1 + C_2\varepsilon^n)\exp[-(C_3 + C_4\varepsilon)T^*] \quad (2)$$

Then, by taking the natural logarithm of Eq. (2), we can obtain Eq. (3):

$$\ln\sigma=\ln(C_1+C_2\varepsilon^n)-(C_3+C_4\varepsilon)T^* \quad (3)$$

Based on the reference strain rate, we substituted the experimental temperatures and different strains of 0.1, 0.15, 0.2, 0.25, 0.3, 0.35, 0.4, 0.45, 0.5 into Eq. (3). Then, the relationship between $\ln\sigma$ and T* can be obtained, as presented in Fig. 2.

By means of the linear fitting to the data in Fig. 2, the obtained intercept I_1 and slope S_1 can be

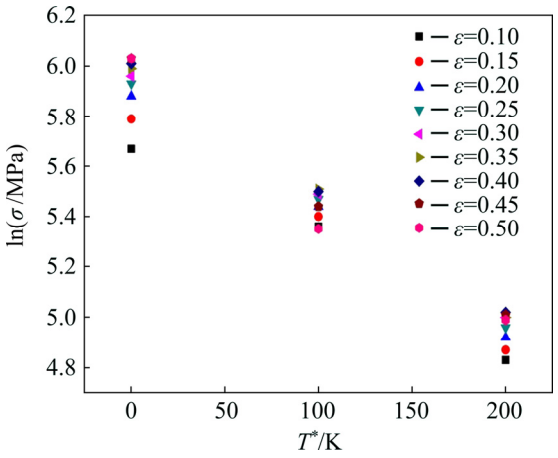

Fig. 2 Plot of ln σ vs T^* at strain rate of 0.01 s^{-1}

expressed as

$$\begin{cases} I_1 = \ln(C_1 + C_2\varepsilon^n) \\ S_1 = -(C_3 + C_4\varepsilon) \end{cases} \quad (4)$$

Taking the natural logarithm to both sides, the first part of Eq. (4) can be rewritten in the form of Eq. (5):

$$\ln(\exp I_1 - C_1) = \ln C_2 + n\ln\varepsilon \quad (5)$$

With the true strain−stress curve at reference temperature and reference strain rate, C_1 can be determined from the yield stress (C_1=222.64). Substituting C_1 into Eq. (5), we can plot the relationship between $\ln(\exp I_1 - C_1)$ and $\ln\varepsilon$, the result is shown in Fig. 3(a), from which we can calculate the intercept and slope values by linear fitting of the above data. Then the value of n and C_2 were determined.

In terms of the second part of Eq. (4), constants of $-C_4$ and $-C_3$ can be gained from the intercept and slope values in Fig. 3(b), which presented the relationship between S_1 and ε.

Finally, taking the natural logarithm to Eq. (1), the following equation can be gained:

$$\ln\sigma = \ln(C_1 + C_2\varepsilon^n) - (C_3 + C_4\varepsilon)T^* + (C_5 + C_6T^*)\ln\dot{\varepsilon}^* \quad (6)\#$$

Substituting the obtained C_1, C_2, C_3, and C_4 into Eq. (6), and performed linear fitting to $\ln\dot{\varepsilon}^*$ and $\ln\sigma$, the slope of this fitted line can be expressed as

$$S_2 = C_5 + C_6T^* \quad (7)$$

Here, C_5 and C_6 can be obtained from the linear fitting of S_2 and T^*. Therefore, all the parameters needed for a modified Zerilli−Armstrong model were gained, and they are summarized in Table 1. Accordingly, the modified Zerilli−Armstrong model of Hastelloy C-276 alloy to describe its hot tensile flow behaviors was established as

$$\sigma = (222.64 + 324.54\varepsilon^{0.50142}) \cdot \exp[-(0.00424 + 0.00197\varepsilon)T^* + (0.04925 + 0.0005625T^*)\ln\dot{\varepsilon}^*] \quad (8)$$

3.2.2 Modified Johnson−Cook model

The modified Johnson−Cook model employed in the present study can be expressed as [21]#

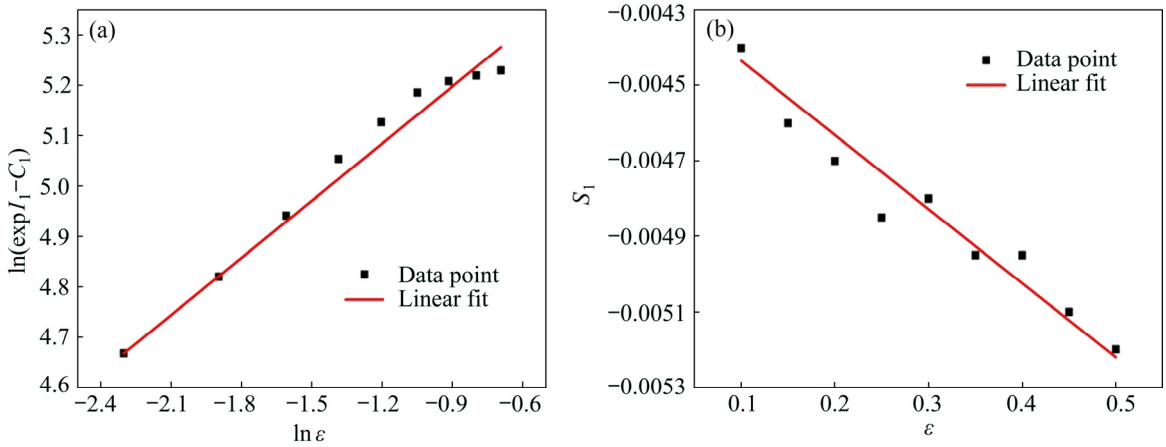

Fig. 3 Relationship between $\ln(\exp I_1 - C_1)$ and $\ln\varepsilon$ (a) and between S_1 and ε (b)

Table 1 Parameters of modified Zerilli−Armstrong model for Hastelloy C-276 alloy

C_1	C_2	C_3	C_4	C_5	C_6	n
222.64	324.54	0.00424	0.00197	0.04925	0.0005625	0.50142

$$\sigma = (A_1 + B_1\varepsilon + B_2\varepsilon^2 + B_3\varepsilon^3)(1 + C\ln\dot{\varepsilon}^*)\cdot \exp[(\lambda_1 + \lambda_2 \ln\dot{\varepsilon}^*)T^*] \quad (9)$$

where A_1, B_1, B_2, B_3, C, λ_1 and λ_2 are material constants.

Similarly, 1223 K and 0.01 s^{-1} are selected as reference temperature and reference strain rate again. When the deformation temperature and strain rate are 1223 K and 0.01 s^{-1}, respectively, the above formula can be expressed as

$$\sigma=(A_1+B_1\varepsilon+B_2\varepsilon^2+B_3\varepsilon^3) \quad (10)$$

Based on the reference temperature and reference strain rate, the stress and strain data obtained from experiments were substituted into Eq. (10). Then, the relationship between σ and ε was plotted in Fig. 4(a), thus, parameters of A_1, B_1, B_2, and B_3 can be gained by the 3rd order polynomial fitting of the plotted curve [34−36].

When the deformation temperature is 1223 K, Eq. (9) can be rewritten as

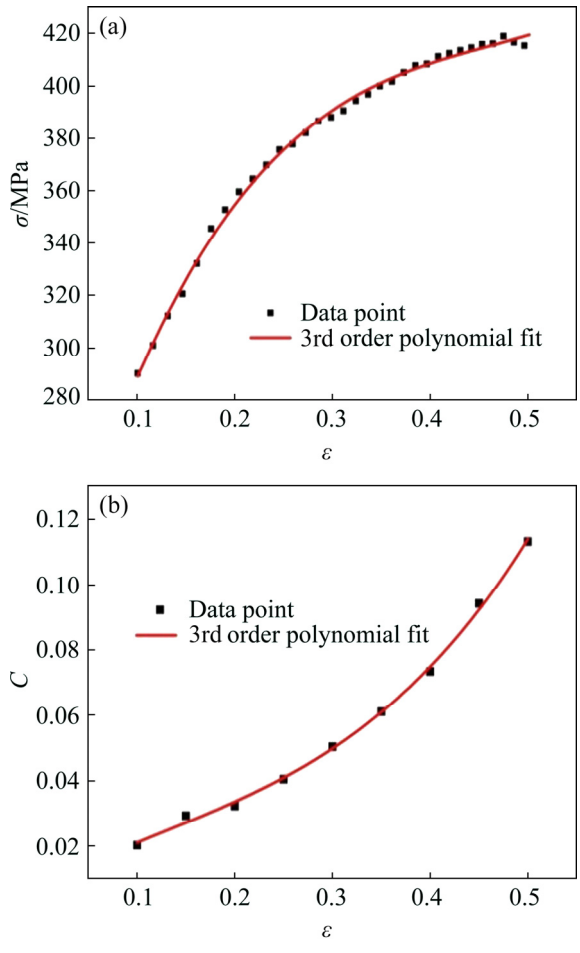

Fig. 4 Relationship between stress and strain at reference temperature and strain rate and its 3rd order polynomial fitting (a) and between C and ε (b)

$$\frac{\sigma}{A_1 + B_1\varepsilon + B_2\varepsilon^2 + B_3\varepsilon^3} = (1 + C\ln\dot{\varepsilon}^*) \quad (11)$$

where C is the material constant that relates to strain, when the deformation temperature is 1223 K, and the strain in the range of 0.1−0.5, the relationship between $\sigma/(A_1+B_1\varepsilon+B_2\varepsilon^2+B_3\varepsilon^3)$ and $\ln\dot{\varepsilon}^*$ can be figured out, the value of material constant C at different strains can be gained from the slope of the corresponding fitting line, and the results are listed in Table 2.

Table 2 Material constant C at different strains

ε	C
0.10	0.02029
0.15	0.02939
0.20	0.03234
0.25	0.04052
0.30	0.05039
0.35	0.06106
0.40	0.07338
0.45	0.09428
0.50	0.11319

As shown in Table 2, it can be seen that C varied with the change of strain. Therefore, a multiple function was defined to describe the relationship between C and ε, according to the characteristics of flow stress for Hastelloy C-276, i.e., $C=C_0(\varepsilon)=C_1+C_2\varepsilon+C_3\varepsilon^2+C_4\varepsilon^3$. Here, C_1, C_2, C_3, and C_4 can be obtained by fitting C and ε, and the result is shown in Fig. 4(b).

When the deformation temperature is 1323 K, Eq. (9) can be expressed as

$$\frac{\sigma}{(A_1 + B_1\varepsilon + B_2\varepsilon^2 + B_3\varepsilon^3)(1 + C\ln\dot{\varepsilon}^*)} = \exp(\lambda T^*) \quad (12)$$

where $\lambda = \lambda_1 + \lambda_2 \ln\dot{\varepsilon}^*$, then taking the natural logarithm of Eq. (12), the following formula was gained:

$$\ln\left[\frac{\sigma}{(A_1 + B_1\varepsilon + B_2\varepsilon^2 + B_3\varepsilon^3)(1 + C_0\ln\dot{\varepsilon}^*)}\right] = \lambda T^* \quad (13)\#$$

For different strain rates, the relationship between $\ln\{\sigma/[(A_1+B_1\varepsilon+B_2\varepsilon^2+B_3\varepsilon^3)(1+C_0\ln\dot{\varepsilon}^*)]\}$ and T^* at different strains can be obtained, as

presented in Fig. 5(a). Then λ at different strain rates can be obtained from the slope of linear fitting lines, and the results are listed in Table 3.

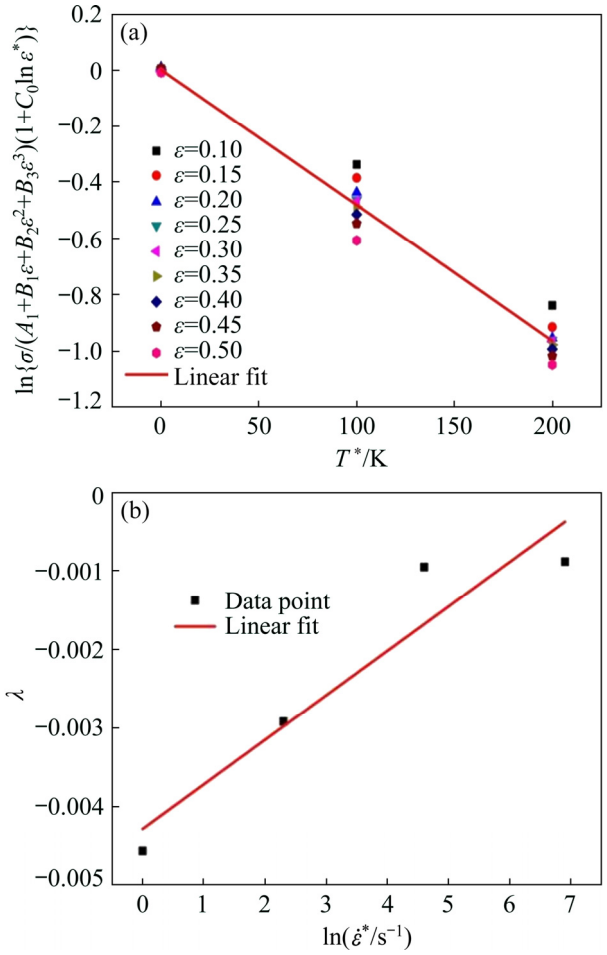

Fig. 5 Relationship between $\ln\{\sigma/[(A_1+B_1\varepsilon+B_2\varepsilon^2+B_3\varepsilon^3)(1+C_0\ln\dot{\varepsilon}^*)]\}$ and T^* at strain rate of 0.01 s^{-1} (a) and between λ and $\ln\dot{\varepsilon}^*$ (b)

Table 3 Material constant λ at different strain rates

$\ln(\dot{\varepsilon}^*/s^{-1})$	λ
0	−0.00482
2.303	−0.00317
4.605	−0.0012
6.908	−0.0011

Finally, λ_1 and λ_2 can be gained by calculating the intercept and slope from the linear fitting of λ and $\ln\dot{\varepsilon}^*$, as shown in Fig. 5(b). Thus, parameters of a modified Johnson−Cook model for Hastelloy C-276 alloy are all determined, which are listed in Table 4.

3.2.3 Arrhenius-type model and its modification

The Arrhenius-type model can be expressed as follows [37]:

$$\dot{\varepsilon}=\begin{cases}A_1\sigma^{n_1}, & \alpha\sigma<0.8\\ A_2\exp(\beta\sigma), & \alpha\sigma<1.2\\ A[\sinh(\alpha\sigma)]^n\exp[-Q/(RT)], & \text{for all }\sigma\end{cases} \tag{14}$$

where A_1, A_2, A, n_1, n, α, β are material constants, Q is the hot deformation activation energy (kJ/mol), R is the universal gas constant (8.31 J/(mol·K)), σ is flow stress. Here, the relationship among α, β and n_1 can be related as $\alpha=\beta/n_1$.

In this work, a Zener−Hollomon parameter (Z) to describe the comprehensive effects of deformation temperature and strain rate on hot deformation behavior of Hastelloy C-276 alloy was introduced, which can be expressed as [38]

$$Z=\dot{\varepsilon}\exp[Q/(RT)] \tag{15}$$

Taking natural logarithm to Eq. (14), and for low-stress level ($\alpha\sigma$<0.8) and high-stress level ($\alpha\sigma$>1.2), we can get

$$\begin{cases}\ln\dot{\varepsilon}=\ln A_1+n_1\ln\sigma\\ \ln\dot{\varepsilon}=\ln A_2+\beta\sigma\end{cases} \tag{16}$$

As an example, the strain rate of 0.3 was used to demonstrate the calculation of material constants for low-stress level. Firstly, we substituted the experimental result of true stress and strain rate under the strain of 0.3 to Eq. (16), and the relationship of $\ln\sigma$ to $\ln\dot{\varepsilon}$ is shown in Fig. 6(a). Then the value of n_1 can be derived by taking the average value of the three linear fitted slopes at different deformation temperatures.

In terms of high-stress level $\alpha\sigma$>1.2 and all σ states, peak stress σ_{p_0} was employed to study the corresponding material constants. Figure 6(b) shows the relationship between σ_{p_0} and $\ln\dot{\varepsilon}$, as well as the linear fitting results under peak stress. Thus, the value of β can be calculated by taking the average value of the three slopes at different deformation temperatures.

Table 4 Parameters of modified Johnson−Cook model for Hastelloy C-276 alloy

A_1	B_1	B_2	B_3	C_1	C_2	C_3	C_4	λ_1	λ_2
181.20	1316.07	−2625.46	1891.79	0.0071	0.16	−0.33	0.86	−0.00454	0.000566

Then, we adopted the natural logarithm to the third part of Eq. (14).

$$\ln[\sinh(\alpha\sigma)]=\frac{\ln\dot{\varepsilon}}{n}+\frac{Q}{nRT}-\frac{\ln A}{n} \quad (17)\#$$

As shown in Eq. (17), by fitting the relationship of $\ln[\sinh(\alpha\sigma)]$ to $\ln\dot{\varepsilon}$, the value of n can be gained from the average slope of the fitting lines at different strains, as presented in Fig. 7(a).

By calculating the average slope of $\ln[\sinh(\alpha\sigma)]$ as a function of T^{-1} under the four kinds of strain rates, as presented in Fig. 7(b), the following Eq. (18) that differentiated from Eq. (17) can be used to calculate Q.

$$Q=Rn\left[\frac{\partial\ln\sinh(\alpha\sigma)}{\partial\ln(1/T)}\right] \quad (18)$$

Based on the obtained n and Q, we can calculate the value of A easily. However, in the above study, we assumed that the influence of strain on flow behavior at elevated temperature of metals is insignificant, and thus we did not take it into account in the above established model, i.e. Eq. (14). Actually, the flow stress was highly influenced by the strain, especially at the beginning of the deformation process. Hence, the effect should be considered when establishing the model. In the present study, a strain-compensated method was used to further improve the accuracy of the prediction.

Here, polynomial fitting to strains was performed based on the material constants that determined from different strains. And as a consequence, a fifth-order polynomial, as presented in Eq. (19), correlates well to represent the influence of strain on material constants (see Fig. 8), and the obtained coefficients of the polynomial functions are listed in Table 5.

$$\begin{cases} n=n_1+n_2\varepsilon+n_3\varepsilon^2+n_4\varepsilon^3+n_5\varepsilon^4+n_6\varepsilon^5 \\ \alpha=\alpha_1+\alpha_2\varepsilon+\alpha_3\varepsilon^2+\alpha_4\varepsilon^3+\alpha_5\varepsilon^4+\alpha_6\varepsilon^5 \\ Q=Q_1+Q_2\varepsilon+Q_3\varepsilon^2+Q_4\varepsilon^3+Q_5\varepsilon^4+Q_6\varepsilon^5 \\ \ln A=A_1+A_2\varepsilon+A_3\varepsilon^2+A_4\varepsilon^3+A_5\varepsilon^4+A_6\varepsilon^5 \end{cases} \quad (19)$$

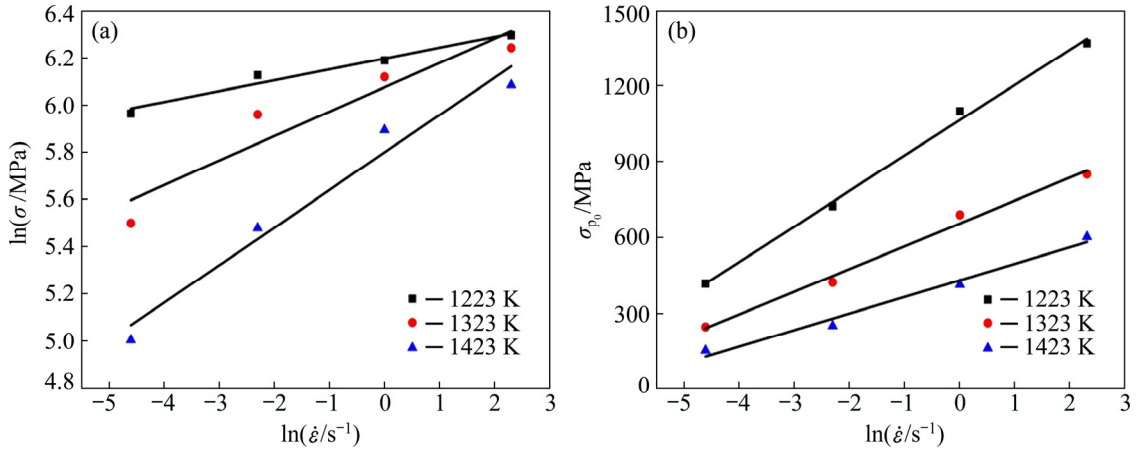

Fig. 6 Relationship between $\ln\sigma$ and $\ln\dot{\varepsilon}$ (a) and between σ_{P_0} and $\ln\dot{\varepsilon}$ (b)

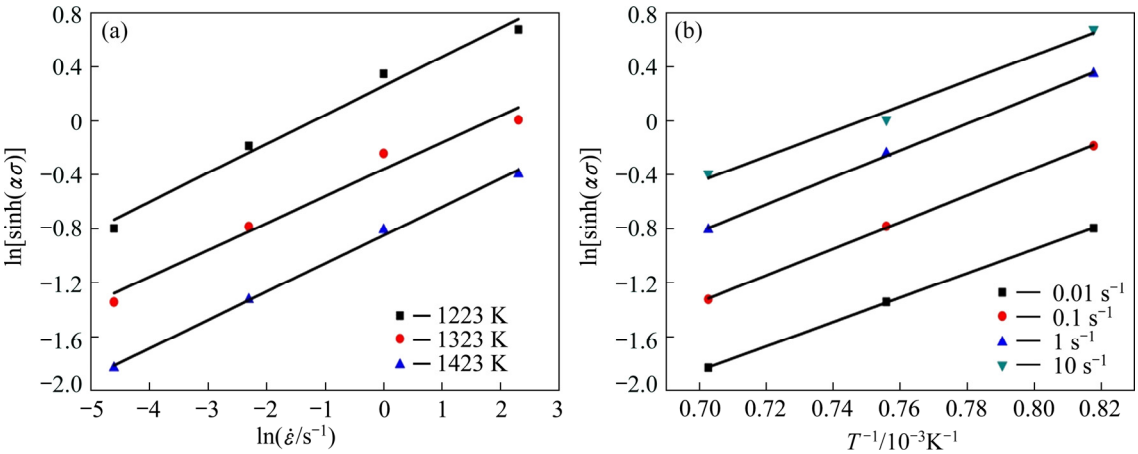

Fig. 7 Relationship between $\ln[\sinh(\alpha\sigma)]$ and $\ln\dot{\varepsilon}$ (a) and between $\ln[\sinh(\alpha\sigma)]$ and T^{-1} (b)

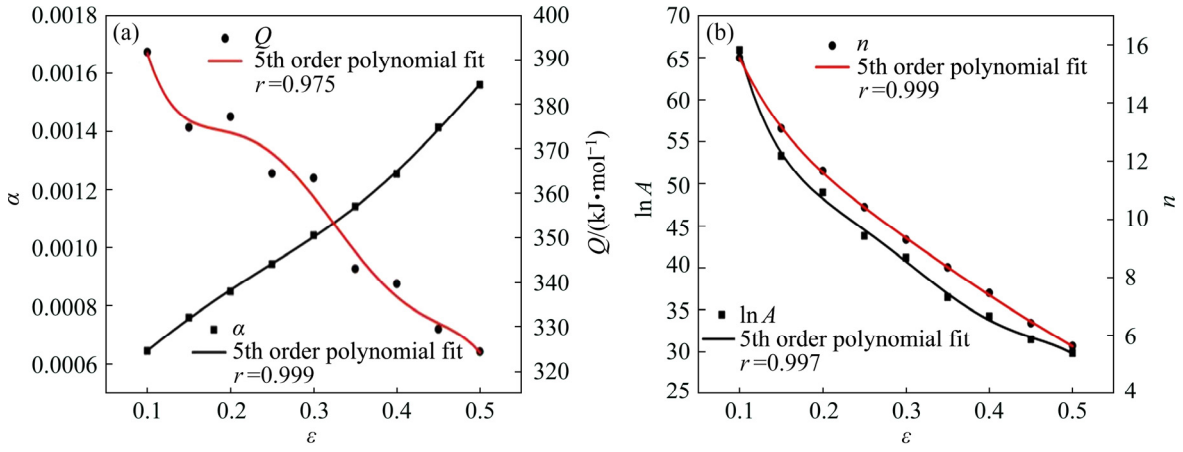

Fig. 8 Variation of α and Q (a), and ln A and n (b)

Table 5 Coefficients of polynomial for α, n, Q and ln A

α	n	Q/(kJ·mol^{-1})	ln A
$\alpha_1=4.457\times10^{-4}$	$n_1=25.643$	$Q_1=593.483$	$A_1=150.620$
$\alpha_2=1.33\times10^{-3}$	$n_2=-157.736$	$Q_2=-4247.070$	$A_2=-1561.493$
$\alpha_3=1.265\times10^{-2}$	$n_3=742.541$	$Q_3=31848.798$	$A_3=9832.143$
$\alpha_4=-7.288\times10^{-2}$	$n_4=-2006.497$	$Q_4=-113363.287$	$A_4=-31540.454$
$\alpha_5=1.621\times10^{-1}$	$n_5=2697.436$	$Q_5=187433.566$	$A_5=48929.091$
$\alpha_6=-1.194\times10^{-1}$	$n_6=-1425.641$	$Q_6=-116869.744$	$A_6=-29236.308$

On the basis of these obtained material constants, the flow stress at a particular strain can be calculated. Also, according to the definition of the hyperbolic law, the flow stress of Hastelloy C-276 can be expressed as a function that includes the Zener−Hollomon parameter, as presented in Eq. (20).

$$\sigma=\frac{1}{\alpha}\ln\{(Z/A)^{1/n}+[(Z/A)^{2/n}+1]^{1/2}\} \tag{20}$$

3.3 Comparisons of three modified constitutive models

After the constitutive models were established, one important step is to assess the accuracy of the above-established models, thus, correlation coefficient (r) was employed in the present study, which could provide details on the linear relationship between experimental data and the predicted data. The r value can be calculated by [36]

$$r=\frac{\sum_{i=1}^{N}\left(\sigma_{\exp}^{i}-\overline{\sigma}_{\exp}\right)\left(\sigma_{\mathrm{p}}^{i}-\overline{\sigma}_{\mathrm{p}}\right)}{\sqrt{\sum_{i=1}^{N}\left(\sigma_{\exp}^{i}-\overline{\sigma}_{\exp}\right)^{2}\sum_{i=1}^{N}\left(\sigma_{\mathrm{p}}^{i}-\overline{\sigma}_{\mathrm{p}}\right)^{2}}} \tag{21}$$

where $\sigma_{\exp}$ is the stress of experimental, σ_{p_0} is the stress of prediction, $\overline{\sigma}_{\exp}$ and $\overline{\sigma}_{\mathrm{p}}$ are average values of $\sigma_{\exp}$ and σ_{p}, respectively, N is the total number of data employed in the calculation.

Then, the experimental and predicted data were substituted into Eq. (21), the results are presented in Fig. 9. The correlation coefficients for the modified Zerilli-Armstrong model, modified Johnson-Cook model and modified Arrhenius-type model are 0.935, 0.968, and 0.984, respectively.

Moreover, the absolute error was also introduced to evaluate the deviation of predicted data from experimental data in the present study. The calculation of absolute error can be expressed as [36]

$$\Delta=\frac{1}{N}\sum_{i=1}^{N}\left|\frac{\sigma_{\exp}^{i}-\sigma_{\mathrm{p}}^{i}}{\sigma_{\exp}^{i}}\right|\times100\% \tag{22}$$

The absolute errors of the modified Zerilli−Armstrong, Johnson−Cook, and modified Arrhenius-type models for Hastelloy C-276 are 13.4%, 10.5% and 6.7%, respectively, which are presented in Fig. 10, together with the correlation coefficient obtained above.

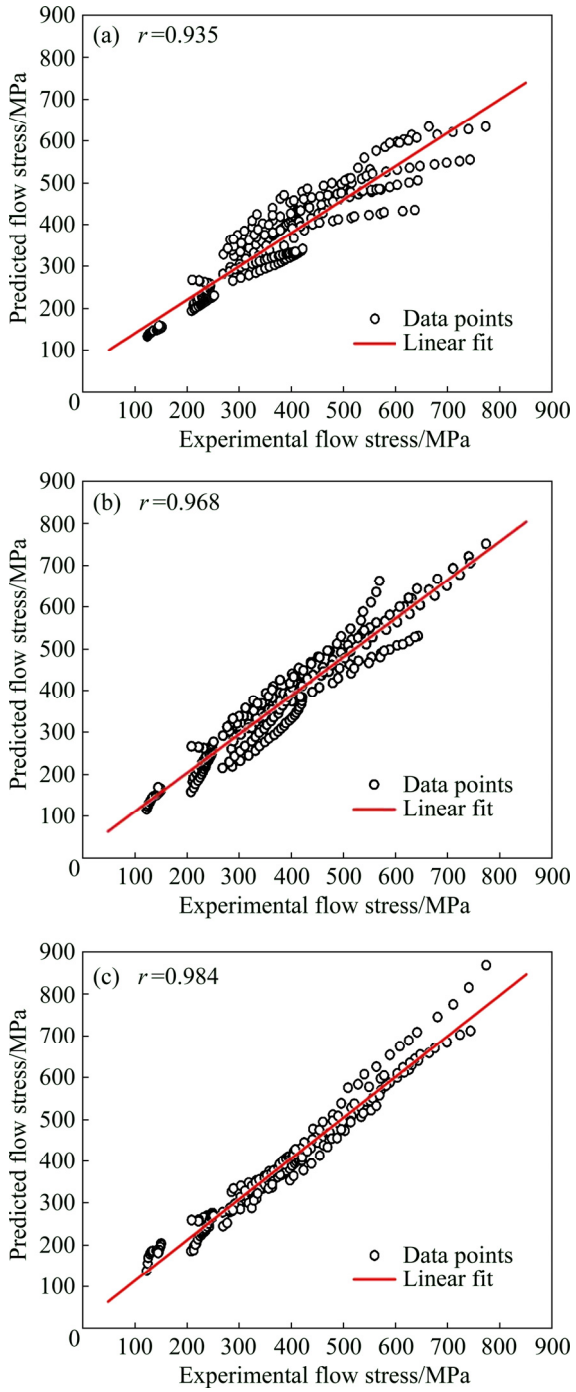

Fig. 9 Correlation between experimental and predicted flow stress values with modified Zerilli−Armstrong model (a), modified Johnson−Cook model (b) and modified Arrhenius-type model (c)

Obviously, the modified Arrhenius-type model possesses the highest correlation coefficient, and the lowest absolute error in comparison with the other two models, indicating that the prediction of flow stress of Hastelloy C-276 with modified Arrhenius-type model has the highest precision in

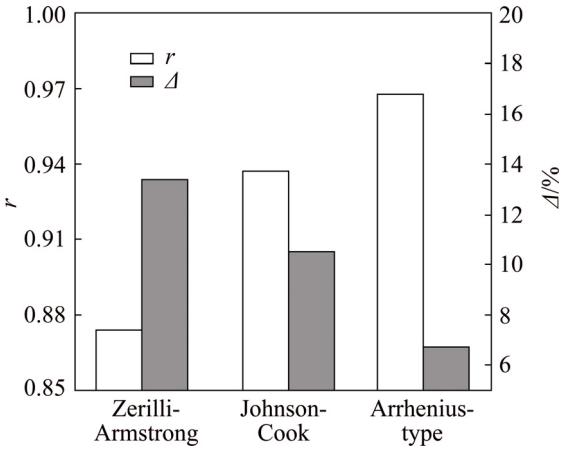

Fig. 10 Comparison of correlation coefficient and absolute error of modified Zerilli−Armstrong model, modified Johnson-Cook model and modified Arrhenius-type model

the present study. Moreover, a comparison of flow stresses between the experimental results and the predicted values with the three obtained constitutive equations was performed, which are presented in Fig. 11. Apparently, it is found that the predictability of the modified Zerilli−Armstrong model at 1223 K is not as good as both the modified Johnson-Cook model and modified Arrhenius-type model. In particular, the predicted stresses with modified Arrhenius-type model were excellently agreement with the experimental results for a wide range of deformation conditions, which agrees well with what the correlation coefficient and absolute error indicated.

On the other hand, it is notable that the modified strain-compensated Arrhenius-type model involves thirteen numbers of material constants, while the number of material constants associated in these two models are both only half of total number that in Arrhenius-type model. Consequently, the time required to determine these material constants of Arrhenius-type model is much longer than that of the modified Johnson-Cook model and modified Zerilli−Armstrong model.

4 Conclusions

(1) The modified Zerilli−Armstrong, modified Johnson-Cook, and strain compensated Arrhenius-type constitutive models of Hastelloy C-276 were established based on the true strain and stress under different tensile conditions. It is found that the

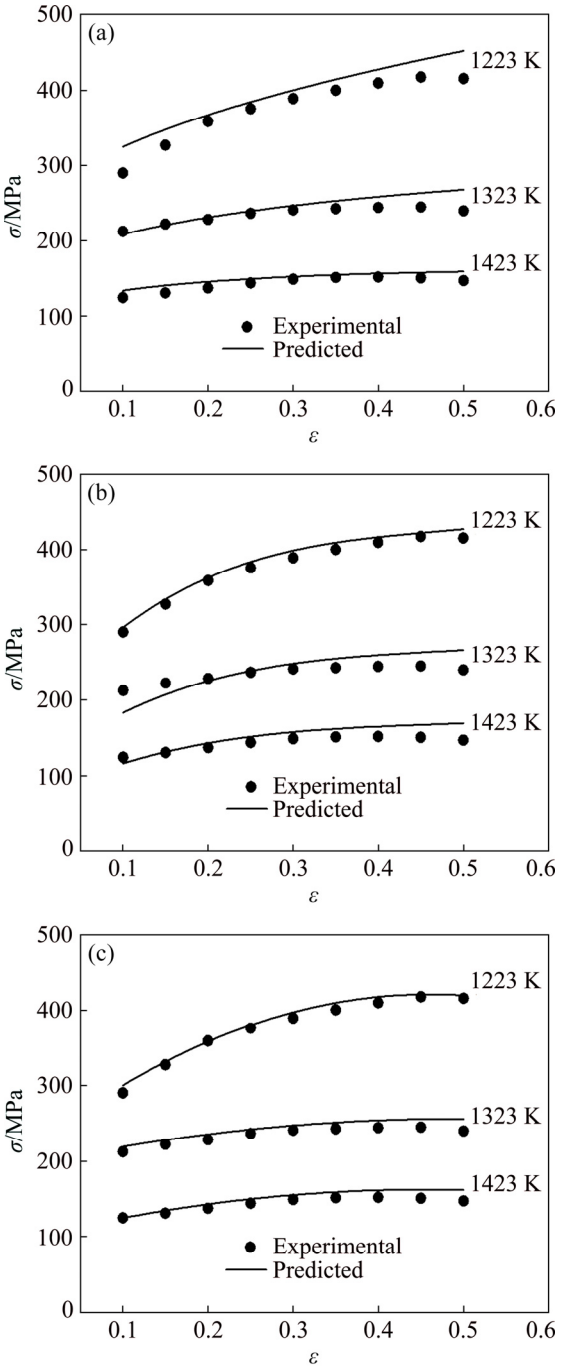

Fig. 11 Comparison between experimental and predicted flow stress with modified Zerilli−Armstrong (a), modified Johnson−Cook (b), and strain-compensated Arrhenius-type equation (c) at strain rate of 0.01 s^{-1}

strain compensated Arrhenius-type model possesses the highest predictability.

(2) The correlation coefficients of the modified Zerilli−Armstrong, Johnson−Cook, and Arrhenius-type constitutive models were calculated to be 0.935, 0.968 and 0.984, while the absolute errors were 13.4%, 10.5% and 6.7%, respectively, which further evidenced the predict precision with the strain compensated Arrhenius-type model to be the highest.

(3) Nevertheless, the determination of the material constants for the strain compensated Arrhenius-type model is much complicated and time-consuming than the modified Johnson-Cook model and Zerilli−Armstrong model, which involves thirteen material constants and almost twice the other two.

References

[1] AL-FALAHI M, FADAEIFARD F, AL-FALAHI M D A, BAHARUDIN B T H T, HONG T S. Surface damages and tool wear mode in end milling of Hastelloy-C276 under dry and wet conditions [J]. Materialwissenschaft und Werkstofftechnik, 2016, 47(12): 1182−1192.

[2] CHEN J, WANG J Z, YAN F Y, ZHANG Q, LI Q A. Corrosion wear synergistic behavior of Hastelloy C276 alloy in artificial seawater [J]. Transactions of Nonferrous Metals Society of China, 2015, 25(2): 661−668.

[3] MA W Y, WANG B Y, LIN J G, TANG X F. Influence of process parameters on properties of AA6082 in hot forming process [J]. Transactions of Nonferrous Metals Society of China, 2017, 27(11): 2454−2463.

[4] WU Y Z, YAN H G, ZHU S Q, CHEN J H, LIU A M, LIU X L. Flow behavior and microstructure of ZK60 magnesium alloy compressed at high strain rate [J]. Transactions of Nonferrous Metals Society of China, 2014, 24(4): 930−939.

[5] KARHAUSEN K, KOPP R, SOUZA M M D. Numerical simulation method for designing thermomechanical treatments, illustrated by bar rolling [J]. Scandinavian Journal of Metallurgy, 1991, 20(6): 351−363.

[6] NOELS L, STAINIER L, PONTHOT J P. Combined implicit/explicit time-integration algorithms for the numerical simulation of sheet metal forming [J]. Journal of Computational & Applied Mathematics, 2004, 168(1−2): 331−339.

[7] MANDAL S, RAKESH V, SIVAPRASAD P V, VENUGOPAL S, KASIVISWANATHAN K V. Constitutive equations to predict high temperature flow stress in a Ti-modified austenitic stainless steel [J]. Materials Science and Engineering A, 2009, 500(1): 114−121.

[8] QIN Y J, PAN Q L, HE Y B, LI W B, LIU X Y, FAN X. Modeling of flow stress for magnesium alloy during hot deformation [J]. Materials Science and Engineering A, 2010, 527(10): 2790−2797.

[9] CHEN F, CUI Z S, LIU J, CHEN W, CHEN S J. Mesoscale simulation of the high-temperature austenitizing and dynamic recrystallization by coupling a cellular automaton with a topology deformation technique [J]. Materials Science and Engineering A, 2010, 527(21): 5539−5549.

[10] KIM J B, SHIN H. Comparison of plasticity models for tantalum and a modification of the PTW model for wide ranges of strain, strain rate, and temperature [J]. International

Journal of Impact Engineering, 2009, 36(5): 746−753.

[11] FOLLANSBEE P S, KOCKS U F. A constitutive description of the deformation of copper based on the use of the mechanical threshold stress as an internal state variable [J]. Acta Metallurgica, 1988, 36(1): 81−93.

[12] GUO Y B, WEN Q, HORSTEMEYER M F. An internal state variable plasticity-based approach to determine dynamic loading history effects on material property in manufacturing processes [J]. International Journal of Mechanical Sciences, 2005, 47(9): 1423−1441.

[13] JOHNSON G R, COOK W H. Fracture characteristics of three metals subjected to various strains, strain rates, temperatures and pressures [J]. Engineering Fracture Mechanics, 1985, 21(1): 31−48.

[14] ZERILLI F J, ARMSTRONG R W. Dislocation-mechanics-based constitutive relations for material dynamics calculations [J]. Journal of Applied Physics, 1987, 61(5): 1816−1825.

[15] SELLARS C M, MCTEGART W J. On the mechanism of hot deformation [J]. Acta Metallurgica, 1966, 14(9): 1136−1138.

[16] ROHR I, NAHME H, THOMA K, ANDERSON C E. Material characterisation and constitutive modelling of a tungsten-sintered alloy for a wide range of strain rates [J]. International Journal of Impact Engineering, 2008, 35(8): 811−819.

[17] NEMAT-NASSER S, GUO W G. Thermomechanical response of DH-36 structural steel over a wide range of strain rates and temperatures [J]. Mechanics of Materials, 2003, 35(11): 1023−1047.

[18] GUPTA A K, ANIRUDH V K, SINGH S K. Constitutive models to predict flow stress in austenitic stainless steel 316 at elevated temperatures [J]. Materials & Design, 2013, 43: 410−418.

[19] WANG Y, ZHOU Y X, XIA Y M. A constitutive description of tensile behavior for brass over a wide range of strain rates [J]. Materials Science and Engineering A, 2004, 372(1): 186−190.

[20] VURAL M, RAVICHANDRAN G, RITTEL D. Large strain mechanical behavior of 1018 cold-rolled steel over a wide range of strain rates [J]. Metallurgical and Materials Transactions A, 2003, 34(12): 2873−2885.

[21] LIN Y C, CHEN X M, LIU G. A modified Johnson–Cook model for tensile behaviors of typical high-strength alloy steel [J]. Materials Science and Engineering A, 2010, 527(26): 6980−6986.

[22] CHIOU S T, CHENG W C, LEE W S. Strain rate effects on the mechanical properties of a Fe−Mn−Al alloy under dynamic impact deformations [J]. Materials Science and Engineering A, 2005, 392(1): 156−162.

[23] LEE W S, LIU C Y. The effects of temperature and strain rate on the dynamic flow behaviour of different steels [J]. Materials Science and Engineering A, 2006, 426(1): 101−113.

[24] SAMANTARAY D, MANDAL S, BHADURI A K, VENUGOPAL S, SIVAPRASAD P V. Analysis and mathematical modelling of elevated temperature flow behaviour of austenitic stainless steels [J]. Materials Science and Engineering A, 2011, 528(4): 1937−1943.

[25] SLOOFF F A, ZHOU J, DUSZCZYK J, KATGERMAN L. Constitutive analysis of wrought magnesium alloy Mg−Al4−Zn1 [J]. Scripta Materialia, 2007, 57(8): 759−762.

[26] LIN Y C, CHEN M S, ZHONG J. Constitutive modeling for elevated temperature flow behavior of 42CrMo steel [J]. Computational Materials Science, 2008, 42(3): 470−477.

[27] CAI J, LI F G, LIU T Y, CHEN B, HE M. Constitutive equations for elevated temperature flow stress of Ti−6Al−4V alloy considering the effect of strain [J]. Materials & Design, 2011, 32(3): 1144−1151.

[28] LI J, LI F G, CAI J, WANG R T, YUAN Z W, XUE F M. Flow behavior modeling of the 7050 aluminum alloy at elevated temperatures considering the compensation of strain [J]. Materials & Design, 2012, 42: 369−377.

[29] KONG Y H, CHANG P P, LI Q, XIE L X, ZHU S G. Hot deformation characteristics and processing map of nickel-based c276 superalloy [J]. Journal of Alloys & Compounds, 2015, 622: 738−744.

[30] ZHANG C, ZHANG L W, SHEN W F, XU Q H, CUI Y. The processing map and microstructure evolution of Ni−Cr−Mo-based C276 superalloy during hot compression [J]. Journal of Alloys & Compounds, 2017, 728: 1269−1278.

[31] ZHANG C, ZHANG L W, CUI Y, GU Y L. Characterization of static recrystallization of a Ni−Cr−Mo-based C276 superalloy in two-stage isothermal compression [J]. Journal of Materials Engineering and Performance, 2018, 27: 6426−6434.

[32] ZHANG C, TANG X L, ZHANG L W, CUI Y. Cellular automaton modeling of dynamic recrystallization of Ni−Cr−Mo-based C276 superalloy during hot compression [J]. Journal of Materials Research, 2019, 1830(34): 3093−3103.

[33] LU Y L, LIU J X, LI X K, LIANG J P, LI Z J, WU G Y. Hot deformation behavior of Hastelly C276 superalloy [J]. Transactions of Nonferrous Metals Society of China, 2012, 22(S1): s84−s88.

[34] WANG X D, PAN Q L, XIONG S W, LIU L L, WANG W Y. Prediction on hot deformation behavior of spray-formed 7055 aluminum alloy via phenomenological models [J]. Transactions of Nonferrous Metals Society of China, 2018, 28(8): 1484−1494.

[35] TAO Z J, FAN X G, YANG H, MA J, LI H. A modified Johnson–Cook model for NC warm bending of large diameter thin-walled Ti−6Al−4V tube in wide ranges of strain rates and temperatures [J]. Transactions of Nonferrous Metals Society of China, 2018, 28(2): 298−308.

[36] LI H Y, LI Y H, WANG X F, LIU J J, WU Y. A comparative study on modified Johnson Cook, modified Zerilli−Armstrong and Arrhenius-type constitutive models to predict the hot deformation behavior in 28CrMnMoV steel [J]. Materials & Design, 2013, 49(8): 493−501.

[37] SHI H, MCLAREN A J, SELLARS C M, SHAHANI R, BOLINGBROKE R. Constitutive equations for high temperature flow stress of aluminium alloys [J]. Metal Science Journal, 1997, 13(3): 210−216.

[38] ZENER C, HOLLOMON J H. Effect of strain rate upon plastic flow of steel [J]. Journal of Applied Physics, 1944, 15(1): 22−32.

修正的 Zerilli−Armstrong、Johnson−Cook 及 Arrhenius 本构模型对 C-276 哈氏合金流变应力的预测

刘 宇[1,2]，李 明[1]，任贤魏[1]，肖政兵[1,3]，张燮义[1]，黄元春[1,2,3,4]

1. 中南大学 轻合金研究院，长沙 410083；
2. 中南大学 有色金属先进结构材料与制造协同创新中心，长沙 410083；
3. 中南大学 高性能复杂制造国家重点实验室，长沙 410083；
4. 中南大学 机电工程学院，长沙 410083

摘 要：为进一步揭示 C-276 哈氏合金的高温流变行为，在温度为 1223~1423 K，应变速率为 0.01~10 s^{-1} 条件下对该合金进行热拉伸测试，并基于修正的 Zerilli−Armstrong 模型、Johnson−Cook 模型和应变补偿的 Arrhenius 模型，分别构建相应的本构方程来反映 C-276 哈氏合金高温流变应力。同时，采用相关系数(r)和绝对误差(Δ)对这 3 个模型的预测精确性进行评价，计算结果显示 Zerilli−Armstrong、Johnson−Cook 和 Arrhenius 本构模型的 r 值分别为 0.935、0.968 和 0.984，Δ 值分别为 13.4%、10.5%和 6.7%。此外，对比分析在 0.1~0.5 应变范围内流变应力的实验值与预测值，结果进一步表明改进的 Arrhenius 模型对 C-276 哈氏合金的高温流变行为具有较好的预测能力。

关键词：C-276 哈氏合金；热拉伸行为；本构模型；流动应力

(Edited by Xiang-qun LI)